Seasonal dynamics of the COS and CO$_2$ exchange of a managed temperate grassland

Felix Maximilian Spielmann[1], Albin Hammerle[1], Florian Kitz[1], Katharina Gerdel[1], Georg Wohlfahrt[1]

[1]Department of Ecology, University of Innsbruck, Innsbruck, 6020, Austria

Correspondence to: Georg Wohlfahrt (Georg.Wohlfahrt@uibk.ac.at)

Abstract. Gross primary productivity (GPP), the CO$_2$ uptake by means of photosynthesis, cannot be measured directly on ecosystem scale, but has to be inferred from proxies or models. One newly emerged proxy is the trace gas carbonyl sulfide (COS). COS diffuses into plant leaves in a fashion very similar to CO$_2$, but is generally not emitted by plants. Laboratory studies on leaf level gas exchange have shown promising correlations between the leaf relative uptake (LRU) of COS to CO$_2$ under controlled conditions. However, *in situ* measurements including daily to seasonal environmental changes are required, to test the applicability of COS as a tracer for GPP at larger temporal scales. To this end, we conducted concurrent ecosystem scale CO$_2$ and COS flux measurements above an agriculturally managed temperate mountain grassland. We also determined the magnitude and variability of the soil COS exchange, which can affect the LRU on ecosystem level. The cutting and removal of the grass at the site had a major influence on the soil flux as well as the total exchange of COS. The grassland acted as a major sink for CO$_2$ and COS during periods of high leaf area. The sink strength decreased after the cuts and the grassland turned into a net source for CO$_2$ and COS on ecosystem level. The soil acted as a small sink for COS when the canopy was undisturbed, but also turned into a source after the cuts, which we linked to higher incident radiation hitting the soil surface. However, the soil contribution was not large enough to explain the COS emission on ecosystem level, hinting to an unknown COS source possibly related to dead plant matter degradation. Over the course of the season, we observed a concurrent decrease of CO$_2$ and COS uptake on ecosystem level. With the exception of the short periods after the cuts, the LRU under high light conditions was rather stable and indicates a high correlation between the COS flux and GPP across the growing season.

1 Introduction

Carbonyl sulfide (COS) is the most abundant sulfur-containing gas in the atmosphere with tropospheric mole fractions of ~500 ppt. Within the atmosphere, COS acts as a greenhouse gas with a 724 times higher direct radiative forcing efficiency as CO$_2$ (Brühl et al., 2012). After reaching the stratosphere, it reacts to sulfur aerosols via oxidation and photolysis, hence contributing to the backscattering of solar radiation and having a cooling effect on Earth's atmosphere (Krysztofiak et al., 2015;Whelan et al., 2018). The intra-seasonal atmospheric COS mole fraction follows the pattern of CO$_2$ as terrestrial vegetation acts as the largest known sink for both species (Montzka et al., 2007;Whelan et al., 2018;Le Quere et al., 2018). However, the relative decrease in ambient mole fraction during summer of the northern hemisphere is 6 times stronger for COS than for CO$_2$ (Montzka et al., 2007) as COS is generally not emitted by plants like CO$_2$, which is released in respiration processes.

The uptake of COS by plants is mostly mediated by the enzyme carbonic anhydrase (CA), but also photolytic enzymes like Ribulose-1,5-bisphosphate-carboxylase/-oxygenase (Rubisco) (Lorimer and Pierce, 1989). This in turn means that COS and CO$_2$ share a similar pathway into leaves through the boundary layer, the stomata and the cytosol, up to their reaction sites. Compared to CO$_2$, COS is processed in a one-way reaction to H$_2$S and CO$_2$ (Protoschill-Krebs and Kesselmeier, 1992;Notni et al., 2007) and therefore not released by plants, with the exception of severely stressed plants (Bloem et al., 2012;Gimeno

39 et al., 2017). That makes COS an interesting tracer for estimating the stomatal conductance and the gross uptake of CO_2,

40 referred to as gross primary production (GPP), on ecosystem level (Asaf et al., 2013;Kooijmans et al., 2017;Kooijmans et al.,

41 2019). However, to estimate GPP using COS, the relative uptake of COS to GPP deposition velocities (LRU) must be known

42 beforehand (see Eq.1), so that GPP can be estimated on the basis of the COS flux.

43 $$LRU = \frac{\frac{F_{COS}}{\chi_{COS}}}{\frac{F_{CO2}}{\chi_{CO2}}}$$ (Eq.1)

44 F_{COS} is the COS leaf flux (pmol m^{-2} s^{-1}), F_{CO2} is the gross CO_2 uptake on leaf level (µmol m^{-2} s^{-1}) and χ_{COS} and χ_{CO2} are the

45 ambient COS and CO_2 mole fractions in ppt and ppm, respectively. Leaf level studies for C_3 plants have estimated the LRU

46 to be around 1.7 with the 95% confidence interval between 0.7 and 6.2 (Whelan et al., 2018;Seibt et al., 2010;Sandoval-Soto

47 et al., 2005). The large spread of the LRU most likely originates from differences between plant species, for example, leaf

48 structure and plant metabolism (Wohlfahrt et al., 2012;Seibt et al., 2010), which questions the applicability of the concept of

49 LRU in real-world ecosystems under naturally varying environmental conditions. It is also known that the LRU is just stable

50 under high light conditions, since the uptake of CO_2 by means of photosynthesis is a light driven process, while CA is able to

51 process COS independently of light conditions (Maseyk et al., 2014;Yang et al., 2018;Stimler et al., 2011). Any model of

52 LRU should therefore reflect diurnal changes in light conditions. Kooijmans et al. (2019) recently discovered that the vapor

53 pressure deficit (VPD) appears to have a stronger control on F_{COS} than on F_{CO2}, in an evergreen needle forest. If generally

54 true, this would add further variability to the LRU and complicating the application of COS to estimate GPP. Besides inter-

55 specific differences in LRU, the question remains unanswered if the LRU is also susceptible to seasonal changes of

56 ecosystems for example, changes in species composition or phenology, which would further complicate the application of

57 COS in carbon cycle research. Maseyk et al. (2014) observed COS emissions on ecosystem scale over a winter wheat field

58 going into senescence, indicating that potentially strong sources of COS could distort LRU.

59 Since CA and other enzymes known to emit or take up COS are also present in microorganisms (Ogawa et al., 2013;Seefeldt

60 et al., 1995;Ensign, 1995;Smeulders et al., 2013;Whelan et al., 2018), recent studies have also quantified the contribution of

61 soils to the COS ecosystem flux (Kooijmans et al., 2017;Spielmann et al., 2019;Maseyk et al., 2014). COS soil fluxes could

62 modify the LRU on ecosystem level and hence inferred GPP, if they are substantial compared to COS canopy fluxes. Similar

63 to the ecosystem fluxes, the soil fluxes could not only be prone to diurnal, but also seasonal changes, depending on the

64 substrate availability, environmental conditions (e.g. soil temperature and moisture) (Liu et al., 2010), substrate quality and

65 quantity, and changes in composition of the microbial communities (Kitz et al., 2019;Meredith et al., 2019). Recent studies

66 have also linked COS soil emissions to abiotic processes dependent on light and/or temperature (Whelan and Rhew,

67 2015;Kitz et al., 2019;Meredith et al., 2018).

68 The goal of our study was to provide new insights into the seasonal variability of COS fluxes on ecosystem, soil and canopy

69 level. To this end, we conducted a 6-month campaign on a managed temperate mountain grassland, measuring ecosystem as

70 well as soil COS fluxes. Since the grassland was cut four times during the campaign, we were able to observe multiple

71 growing cycles and investigate the diel and seasonal changes of the COS fluxes and the LRU in this highly dynamic

72 ecosystem. We hypothesize that (H1) the grassland, given its large CO_2 uptake capacity (Wohlfahrt et al. 2008), is a major

73 sink for COS and that the sink strength decreases over the course of the season, (H2) the drying of the cut grass leads to a

74 release of COS, (H3) the LRU will change after the cuts, due to stressed plants and drying plant parts in the field, but is

75 otherwise stable, (H4) the cuts turn the soil into a COS source, due to the larger amount of light reaching the soil surface

76 (Kitz et al., 2017), but once a reasonably high leaf area index (LAI) has developed, COS is taken up by soil.

2 Methods

2.1 Study site and period

The study was conducted at an intensively managed mountain grassland in the municipal territory of Neustift (Austria) in Stubai valley (FLUXNET ID: AT-Neu; doi: 10.18140/FLX/1440121). The grassland is situated at an elevation of 970 m a.s.l. in the middle of the flat valley bottom. The soil was classified as Fluvisol with an estimated depth of 1 m with the majority of roots located within the first 10 cm. Measurements were conducted between June 01, 2015 and October 31, 2015 (183 days). The vegetation was described as Pastincao-Arrhenatheretum and consisted mainly of *Dactylis glomerata, Festuca pratensis, Alopecurus pratensis, Trisetum flavescens, Ranunculus acris, Taraxacum offcinale, Trifolium repens, Trifolium pratense,* and *Carum carvi (Kitz et al., 2017)*. During the campaign, the grassland was cut four times (June 02/ July 07/ August 21/ October 01, 2015) and the biomass left to dry on the field for up to one day, before being removed as silage. Each year, the field site was fertilized with solid manure and cattle slurry (Hörtnagl et al., 2018) at the end of the season (October 07, 2015).

2.2 Leaf area index

The LAI was estimated from assessments of the average canopy height, which were related to destructive LAI measurements, using the following sigmoid function:

$$LAI = 1 \Big/ \left(1 + \exp\left(-(a_1 DOY + a_2)\right)\right)(b_1 - b_2) \tag{Eq.2}$$

where DOY is the day of the year and a1, a2, b1 and b2 are factors that were optimized for each growing period, for example, before the first cut, between cuts and after fourth cut (Wohlfahrt et al., 2008). Additionally, biomass samples were taken at 15 occasions, to assist with the LAI calculation.

2.3 Mole fraction measurements

The CO_2 (χ_{CO2}) and COS (χ_{COS}) mole fractions were measured using a Quantum Cascade Laser (QCL) Mini Monitor (Aerodyne Research, Billerica, MA, USA) at a wavenumber of ca. 2056 cm^{-1} and at a frequency of 10 Hz. To minimize the effect of air temperature (T_{air}) changes on the instrument, we placed it in an insulated box which in turn was located in a climate controlled instrument hut (30°C). The cooling of the laser was achieved by a chiller (ThermoCube 400, Solid State Cooling Systems, Wappinger Falls, NY, USA).

We used ¼ inch Teflon™ tubing, stainless steel fittings (SWAGELOK, Solon, OH, USA and FITOK, Offenbach, HE, Germany), Teflon Filters (Savilex, EdenPrarie, MN, USA) as well as COS-inert valves (Parker-Hannafin, Cleveland, OH, USA) to ensure that only materials known not to interact with COS were used for the measurement and calibration airflow. Since the data of the QCL and the sonic anemometer were saved on two separate PCs, a network time protocol software (NTP, Meinberg, NI, Germany) was used to keep the time on both devices synchronized. We corrected known χ_{COS} drift issues of the QCL (Kooijmans et al., 2016) by doing half hourly calibrations for 1 min with a gas of known χ_{COS}. The gas cylinders (working standards) used for the calibrations were either pressurized air (UN 1002) or nitrogen (UN 1066), which were cross-compared (when working standard cylinders were full and close to empty) to an Aculife-treated aluminum pressurized air cylinder obtained from the National Oceanic & Atmospheric Administration (NOAA). The latter was analyzed by the central calibration laboratory of NOAA for its χ_{COS} using gas chromatography with mass spectrometric detection (GC-MS) on April 06, 2015. We then linearly interpolated between the offsets of the half hourly calibrations and used the retrieved values to correct the high frequency COS data. Due to issues with the scale gas cylinder, no absolute concentrations were available before June 16, 2015. To increase the amount of available data for the first post cut period, we

115 extrapolated the COS mole fractions to the day of the 1st cut. This was done on the basis of the measured CO_2 mole fractions

116 and the mean half hourly ratio of the ambient CO_2 to COS mole fractions retrieved between June 16 and June 18, 2015.

2.3.1 Mole fraction measurements within the canopy

118 In order to investigate the χ_{COS} within the canopy, we used a multiplexer and 8 ¼ inch Teflon™ tubes to measure the χ_{COS} at

119 8 heights within and above the canopy i.e. at 2, 5, 10, 20, 30, 40, 50 & 250 cm height above ground with a tube length of

120 15 m for each height. The upper two intakes were located at the eddy covariance measurement and canopy height,

121 respectively. Each height was measured for 1 min at 1 Hz and 2 l min⁻¹, while the other lines were each flushed at 2 l min⁻¹.

122 The χ_{COS} drift was also corrected by doing half hourly calibrations (see section 2.3).

2.4 COS soil fluxes

2.4.1 Soil chamber setup

126 To quantify soil COS fluxes, we installed four stainless steel (SAE grade: 316L) rings 5 cm into the soil. They remained on

127 site for 112 days (June 10, 2015 – September 30, 2015). Two additional rings were installed on August 31, 2015 and the

128 October 02, 2015 to examine any long-term effects of the ring placement and to replace the original rings for the

129 measurements in September and October. The aboveground biomass within each ring was removed at the day of installation

130 and again at least one day prior to each measurement day. The roots within as well as the vegetation surrounding the rings

131 were not removed and natural litter was left in place. At days without measurements the soil within the rings was covered by

132 fleece to prevent it from drying out.

133 To measure the soil fluxes, a transparent fused silica-glass chamber with a volume of approximately 4155 cm³ (Kitz et al.,

134 2017) was placed into the water filled channel of the steel rings, while air was sucked through the chamber to the QCL at a

135 flow rate of 1.5 l min⁻¹. The chamber χ_{COS} was then compared with the ambient χ_{COS} above the chamber, using a second inlet

136 to which we switched before the chamber measurement and after reaching stable readings inside the chamber. The intake

137 height of the ambient as well as the inlet of the chamber air were located at 0.12 m above the ground and thus within the

138 canopy height with the exception of measurements right after the cuts (see cutting dates in Section 2.1). Overall, 243

139 chamber measurements were conducted over the course of the campaign including day and nighttime measurements.

140 Additional manual measurements included a hand-held sensor (WET-2, Delta-T Devices, Cambridge, England) to measure

141 soil water content (SWC) and soil temperature (T_{soil}) at a soil depth of 5 cm simultaneously with the soil chamber

142 measurements next to the rings.

2.4.1 COS soil flux calculation

144 The COS soil flux was calculated using the following equation:

145 $$F = {q(\chi_{cos2} - \chi_{cos1})}/{A} \qquad \text{(Eq.3)}$$

146 where F is the COS soil flux (pmol m⁻² s⁻¹), q denotes the flowrate in (mol s⁻¹), χ_{COS2} and χ_{COS1} are the chamber and ambient

147 χ_{COS} in ppt, respectively and A the soil surface area (0.032 m²) covered by the chamber. A more detailed description can be

148 found in Kitz et al. (2017).

2.4.2 COS soil exchange modelling

150 Due to the removal of the aboveground biomass and the consequent higher shortwave radiation reaching the soil surface in

151 the chambers, compared to the soil below the canopy, we simulated the soil COS exchange for natural conditions. The soil

152 flux was modelled using our measured soil fluxes and additionally retrieved soil and meteorological data - T_{soil}, soil water

153 content (SWC) at 5 cm depth next to the chambers and incident shortwave radiation reaching the soil surface ($R_{SW-soil}$) - as

154 input for a random forest regression model (Liaw and Wiener, 2002). The soil fluxes were modelled on half hourly basis for

155 the whole duration of the measurement campaign to calculate the COS canopy fluxes from the difference of the COS

156 ecosystem and soil fluxes. To this end we used the scikit-learn (sklearn Ver. 0.19.1) package, the pandas library and the

157 Python Software Distribution Anaconda (Ver. 5.2.0) in the command shell Ipython (Ver. 6.4.0) based on the Programming

158 language Python (Ver. 3.3.5). We used the Beer-Lambert law to model R_{SW_soil} under undisturbed conditions as the

159 aboveground vegetation was removed to measure the COS exchange of bare soil:

160 $$R_{SW-soil} = R_{SW} \exp(-K \, LAI) \hspace{3cm} (Eq.4)$$

161 where $R_{SW-soil}$ (Wm^{-2}) is the shortwave radiation (SW) reaching the soil surface, R_{SW} is the incoming SW radiation reaching

162 the top of the canopy, LAI is the plant area index (Eq. 2) and K is the canopy extinction coefficient assuming a spherical leaf

163 inclination distribution (Wohlfahrt et al., 2001), which was calculated using the following equation:

164 $$K = \frac{1}{2\cos(\psi)} \hspace{4cm} (Eq.5)$$

165 where ψ is the zenith angle of the sun in radians.

166

167 A random forest with 1000 trees was grown which resulted in an out of bag (OOB) score of (0.82). The OOB score can be

168 interpreted as a pseudo-R2 and is widely used in random forest analyses (regression and classification), especially in the

169 absence of a proper test dataset. It uses the data not seen by the trees (random forest uses bootstrapping) as a test dataset. The

170 optimal input parameters, including maximum tree depth, were determined with the function GridSearchCV from the sklearn

171 package.

2.5 Ecosystem fluxes

2.5.1 Setup for ecosystem fluxes

174 The COS, CO_2 and H_2O ecosystem fluxes were obtained using the eddy covariance method (Aubinet et al., 1999;Baldocchi,

175 2014). We used a 3-axis sonic anemometer (Gill R3IA, Gill Instruments Limited, Lymington, UK) to obtain high-resolution

176 data of the 3 wind components. The intake of the tube for the eddy covariance measurements was installed in close

177 proximity to the sonic anemometer and insulated as well as heated above T_{air} to prevent condensation within the tube. The air

178 was sucked to the QCL at a flowrate of $7 \, l \, min^{-1}$ using a Vacuum Pump (Agilent Technologies, CA, USA).

2.5.2 Ecosystem flux calculation

180 In a first step we used a self-developed software to determine the time lag, introduced by the separation of tube intake and

181 the sonic anemometer and the tube length, between the QCL and sonic dataset (Hortnagl et al., 2010). The data were then

182 processed using the software EdiRe (University of Edinburgh, UK) and Matlab2019a (MathWorks, MA, USA). We used the

183 laser drift corrected χ_{COS} data and linear detrending to process the data before following the procedure to correct for sensor

184 response, tube attenuation, path averaging and sensor separation following Gerdel et al. (2017). The random flux uncertainty

185 was calculated following Langford et al. (2015).Nighttime NEE and COS fluxes were filtered for periods of low friction

186 velocity (u*). We determined the u* threshold ($0.19 \, m \, s^{-1}$) by running the change point detection algorithm of Barr et al.

187 (2013) on nighttime NEE (Fig. S9) and applied it on the nighttime NEE as well as the COS fluxes.

188 We estimated the COS canopy flux from the difference between the measured COS ecosystem and the modelled COS soil

189 flux.

2.5.3 Flux partitioning and leaf relative uptake

The GPP on ecosystem level was determined using the FP+ model put forward by Spielmann et al. (2019). The model estimates the GPP on the basis of nighttime net ecosystem exchange (NEE) measurements of CO_2 that are assumed to provide the temperature response of the ecosystem respiration (RECO) as well as a light dependency curve to estimate GPP based on the daytime NEE (Lasslop et al., 2010):

$$NEE = \frac{\alpha\beta R_{PAR}}{\alpha R_{PAR}+\beta} + rb\, e^{E_0\left(\frac{1}{T_{ref}-T_0}-\frac{1}{T_{air}-T_0}\right)} \tag{Eq.6}$$

where α denotes the canopy light utilization efficiency (μmol CO_2 μmol^{-1} photons), β the maximum CO_2 uptake rate of the canopy at light saturation (μmol CO_2 m^{-2} s^{-1}), R_{PAR} the incoming photosynthetic active radiation (μmol m^{-2} s^{-1}), rb the ecosystem base respiration (μmol m^{-2} s^{-1}) at the reference temperature T_{Ref} (°C), which is set to 15°C, T_{air} (°C) refers to the air temperature and E_0 (°C) to the temperature sensitivity of RECO. T_0 was kept constant at -46.02°C. We did not use the VPD modifier of beta put forward by Lasslop et al. (2010) as its value could not be estimated with confidence. We determined the parameter E_0 by using nighttime data minimizing the root squared mean error. For the determination of the remaining five unknown model parameters of the two flux partitioning models we used DREAM, a multi-chain Markov Chain Monte Carlo algorithm (for more detail see Spielmann et al. (2019)). We calculated the parameters for ~15 day windows but adjusted them to not overlap with a cut of the grassland.

The ecosystem relative uptake (ERU) was calculated using Eq. 1 substituting the GPP with the NEE and using the COS ecosystem flux for F_{COS}.

The FP+ model by Spielmann et al. (2019) extends the daytime FP (Eq.6) to also estimate the COS ecosystem fluxes by linking the GPP resulting from the first part on the right-hand side of Eq.6 with the COS exchange through:

$$F_{COSmodel} = \frac{GPP\, LRU\chi_{COS}}{\chi_{CO2}} \tag{Eq.7}$$

developed by Sandoval-Soto et al. (2005), where $F_{COSmodel}$ is the modelled COS flux (pmol m^{-2} s^{-1}), χ_{COS} (ppt) and χ_{CO2} (ppm) are the measured ambient mole fractions of COS and CO_2 respectively and LRU (-) is the leaf relative uptake rate:

$$LRU = \iota\, e^{\left(\frac{\kappa}{R_{PAR}}\right)} \tag{Eq.8}$$

where ι (-) corresponds to the LRU at high light intensity and the parameter κ (μmol m^{-2} s^{-1}) governs the increase of LRU at low light conditions. While mathematically ι is only obtained at infinitely high PAR, in practice above about 700 μmol m^{-2} s^{-1} PAR (Kooijmans et al., 2019) only insignificant change is reported in other studies (Stimler et al., 2011). The light dependency of LRU originates from the fact that the COS uptake by the enzyme CA is light-independent, while the CO_2 uptake by Rubisco depends on solar radiation absorbed by leaf chlorophyll (Whelan et al., 2018;Kooijmans et al., 2019;Wohlfahrt et al., 2012).

The method stated above infers LRU solely on the basis of ecosystem scale fluxes, whereas other studies typically use branch/leaf chamber measurements (Yang et al., 2018) to determine the relationship between the COS and CO_2 uptake rates.

2.5.4 Linear perturbation analysis

The relative contribution of the parameters GPP, $F_{COSmodel}$, χ_{CO2} and χ_{COS} that drive ι (Eq. 7) were estimated through a linear perturbation analysis (Stoy et al., 2006).

The changes in ι ($\delta\iota$) between the target and the reference window (before the 2nd cut, i.e. June 18, 2015-July 07, 2015) are considered the total derivative of Eq. 7 and can be represented by a multivariate Taylors's expansion where the higher-order terms are neglected in this first-order analysis:

$$\delta\iota = \frac{\partial\iota}{\partial F_{COSmod}}dF_{COSmod} + \frac{\partial\iota}{\partial\chi_{COS}}d\chi_{COS} + \frac{\partial\iota}{\partial GPP}dGPP + \frac{\partial\iota}{\partial\chi_{CO2}}d\chi_{CO2} \tag{Eq.9}$$

The relative contributions of the parameters were determined by computing the partial derivatives of Eq. 7.

229 $$\frac{\partial \iota}{\partial F_{COSmod}} = \frac{\chi_{CO2}}{\chi_{COS}GPP} \qquad \text{(Eq.10)}$$

230 $$\frac{\partial \iota}{\partial \chi_{COS}} = \frac{-\chi_{CO2}F_{COSmod}}{\chi_{COS}^2 GPP} \qquad \text{(Eq.11)}$$

231 $$\frac{\partial \iota}{\partial GPP} = \frac{\chi_{CO2}F_{COSmod}}{\chi_{COS}GPP^2} \qquad \text{(Eq.12)}$$

232 $$\frac{\partial \iota}{\partial \chi_{CO2}} = \frac{F_{COSmod}}{\chi_{COS}GPP} \qquad \text{(Eq.13)}$$

233

234 2.6 Ancillary data

235 Supporting meteorological measurements included T_{air} (RFT-2, UMS, Munich, GER), T_{soil} (TCAV, Campbell Scientific,

236 Logan, UT, USA), SWC (ML2x, Delta-T Devices, Cambridge, UK), incident solar radiation (CNR-1, Klipp and Zonen,

237 Delft, NLD), incident photosynthetic active radiation (PAR) (BF2H, Delta-T Devices Ltd, Cambridge, UK) and the

238 Normalized Difference Vegetation Index (NDVI) sensor (SRS-NDVI, Meter, Pullman, WA, USA). The data were recorded

239 throughout the whole season as 1 min values and stored as half-hourly means and standard deviations.

240 3 Results

241 3.1 Environmental conditions

242 Air temperature ranged between -2 °C and 33 °C with a mean of 13 °C during the study period from 15th of May to first of

243 November (Fig. 1). While the majority of precipitation (total 360.5 mm) fell as rain, we observed an exceptionally late snow

244 event on the 20th of May, which did not melt for almost two days (Fig. 1). Although the VPD reached values of above 2 kPa

245 during 25 days, and plant available water dropped below 50 % on 111 days during the campaign (Fig. 1), we did not observe

246 any relationship with COS (see Fig S1-S2). Due to the removal of the aboveground biomass, the cuts reduced LAI. They

247 also reduced the normalized difference vegetation index (NDVI) (Fig. 1), which is a measure of canopy greenness (Tucker,

248 1979). The NDVI further decreased in the subsequent days as a consequence of dying plant parts remaining at the field site

249 (Fig 2 panels a-c). This can also be observed in the webcam photos (Photo S1-S3).
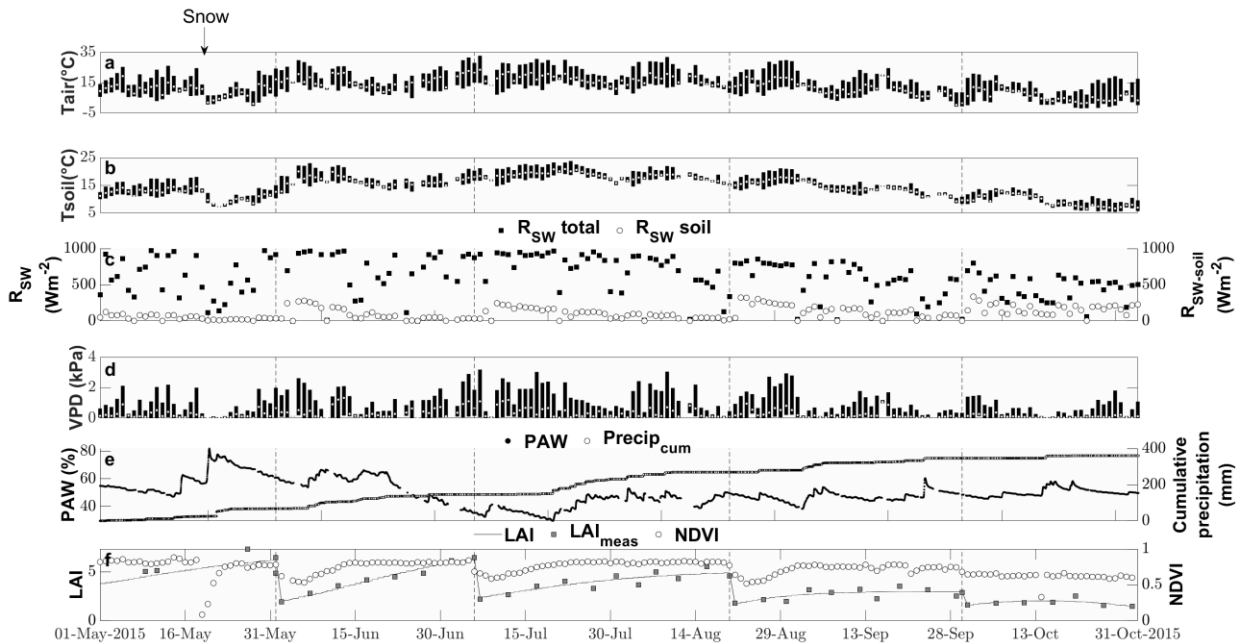
250

251 **Figure 1.** Seasonal cycle of ancillary variables. Daily minimum, maximum and median (a) air and (b) soil temperatures (°C) indicated by
252 the lower and upper end of the bars and the white circle, respectively. (c) Daily maximum incident shortwave radiation (W m^{-2}) reaching

253 the top of the canopy (black squares) and reaching the soil surface (white circles). (d) Daily minimum, maximum and median vapor
254 pressure deficit (kPA) indicated by the lower and upper end of the bars and the white circle, respectively. (e) Plant available water (%)
255 depicted by black squares and cumulative precipitation (mm) depicted by open circles. (f) Modelled leaf area index (black lines), measured
256 LAI (grey squares) and normalized difference vegetation index (open circles).

257
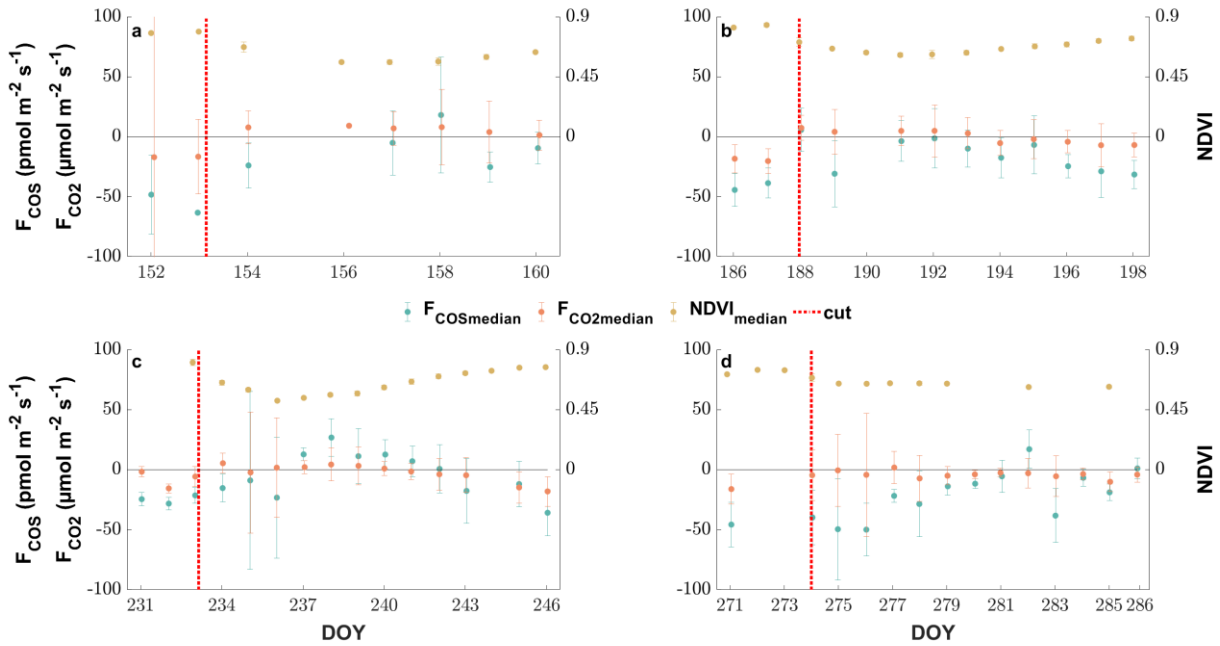
Figure 2: The response of the daily midday medians of NDVI (yellow circles), COS (blue circles) and CO_2 (red circles) ecosystem fluxes
around the 4 cutting events (a-d) of the grassland. The errorbars depict the respective median absolute deviations. The cuts are marked by a
red dashed line.

3.2 COS mole fractions above and within the canopy

While the canopy depleted the ambient χ_{COS} during day as well as nighttime, we found that the χ_{COS} reached values as low as
134 ppt (depletion of 102 ppt with respect to the mole fraction at canopy height) during nighttime (see Fig. 3) at the bottom
of the canopy in contrast to the midday χ_{COS}, which only went down to 389 ppt (depletion of 125 ppt with respect to the mole
fraction at canopy height). We observed a decrease in χ_{CO2} (up to 26 ppm) within the most upper layers of the canopy
compared to χ_{CO2} at canopy height during daytime, while χ_{CO2} increased within the lowest layers compared to χ_{CO2} at the
canopy height due to soil respiration. The above canopy χ_{COS} increased considerably starting at the onset of the day and
reached 587 ppt at 4 p.m. with a steep increase until 11 a.m. Over the course of the season the midday ambient χ_{COS}
decreased from 500 ±28 ppt from mid-June to mid-July to 405±29 ppt in October with the trend of increasing χ_{COS} starting at
the end of September (see Fig. S6).
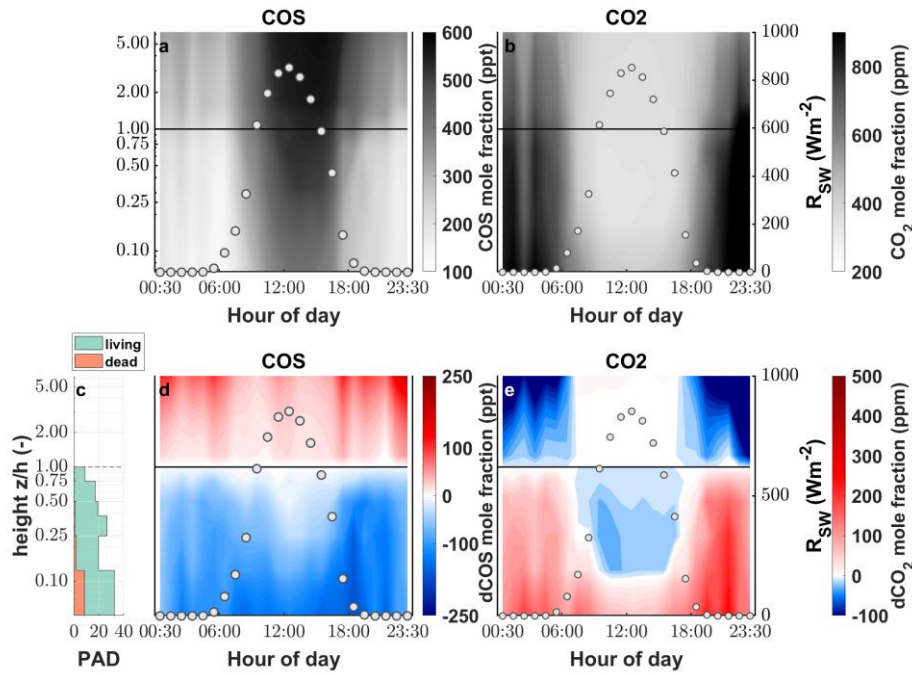
Figure 3. Vertical gradient of the (a) COS and (b) CO_2 mole fraction (ppt and ppm, respectively) depicted by the background color between the soil and the eddy covariance tower at 250 cm for one day. The left y axis shows the log of the measurement divided by the canopy height (z/h). The white circles depict the incoming shortwave radiation (R_{SW}) in (W m^{-2}). Plant area density (PAD) split into living (green) and dead (brown) plant material (c). Vertical gradient of the difference between the mole fraction at canopy height and each measurement height for (d) COS and (e) CO_2.

3.3 COS soil flux

The fluxes resulting from the soil chamber measurements ranged from -6.3 to 40.9 pmol m^{-2}s^{-1}, with positive fluxes denoting emission (see Fig. 4 panel d).

During nighttime (RSW = 0, n = 43), 74.4 % of the COS fluxes were negative, implying that the soil of the grassland acted as a net sink for COS (range of -4.4 to 6.9 pmol m^{-2}s^{-1}), whereas soils transitioned to a source in 88.5 % of all daytime measurements ($R_{SW} > 0$, n = 200), reaching the highest fluxes of 40.9 pmol m^{-2}s^{-1} during midday (see Fig. 4 a-c and Fig. S3). This diel pattern was maintained over the course of the season, however with decreasing maximum COS source strength of the soil towards the end of the season (Fig. 4 a-c and Fig. S3). The random forest regression revealed that the most important variable for predicting the soil fluxes was the incident shortwave radiation reaching the soil surface ($R_{SW-soil}$), accounting for more than 73.53 % of the total variance explained by the final model, while SWC and T_{soil} only accounted for 17.84 % and 8.62 %, respectively. The fast response of the COS soil fluxes to changes in R_{SW} can be seen in Fig. 4 a, where we observed a decrease of $R_{SW-soil}$ as well as the COS soil flux during a cloudy period, even when the soil temperature still increased. Soil fluxes estimated with the random forest regression ranged from -1.3 to 5.0 pmol m^{-2}s^{-1}, reflecting the fact that under real-world conditions very little solar radiation reaches the soil surface. (Fig. 4 e). The resulting emissions peaked during daytime shortly after the cuts when a high proportion of incident radiation was reaching the soil surface, while simulated nighttime fluxes were dominated by uptake (in 93 % of all cases) for the whole season.
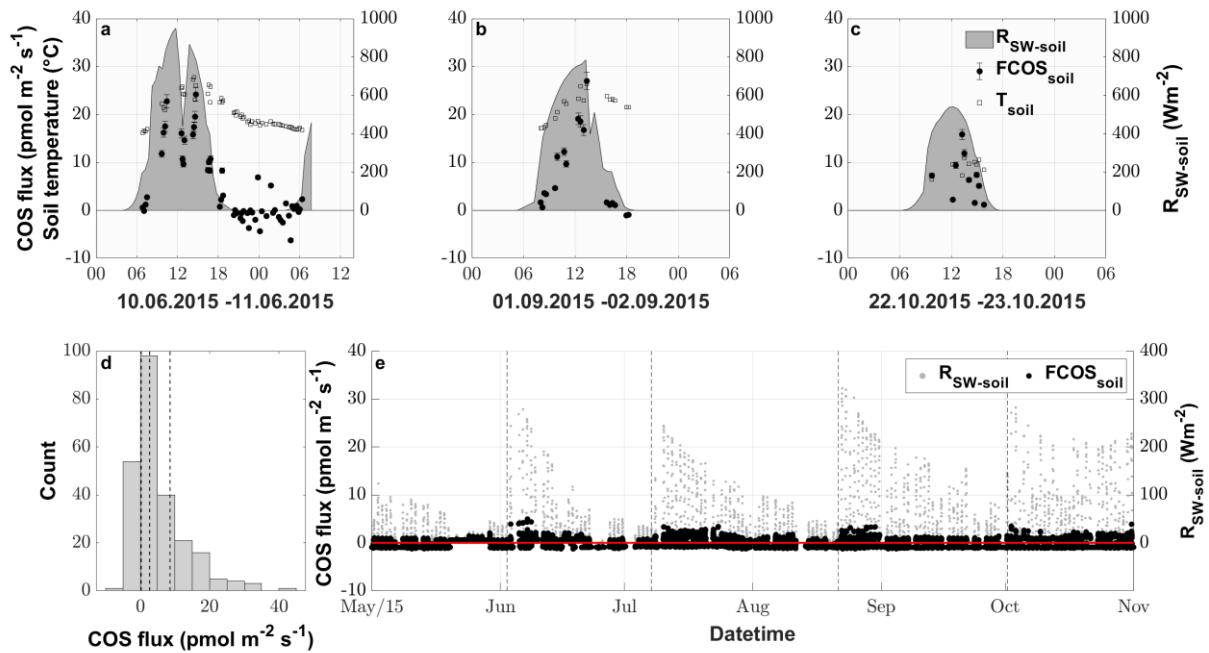
Figure 4. COS soil fluxes (pmol m^{-2}s^{-1}) originating from manual chamber measurements of three selected days (a), (b) and (c) depicted by black circles, incident shortwave radiation reaching the soil ($R_{SW\text{-}soil}$) depicted by the gray area and soil temperature (T_{soil}) depicted by empty black bordered squares. (d) Histogram of all conducted COS soil chamber observations with the dashed vertical lines depicting the 25, 50 and 75% quantile. (e) Season plot of the modelled COS soil fluxes ($F_{COSsoil}$) depicted by the black circles, incident shortwave radiation reaching the soil surface ($R_{SW\text{-}soil}$) depicted by grey circles and the black dashed lines depicting the cuttings of the grassland.

3.4 COS and CO$_2$ ecosystem-scale fluxes

The grassland acted as a net sink for COS during the majority of our study period with 80 % of the COS ecosystem fluxes between -56.0 pmol m^{-2}s^{-1} and -4.5 pmol m^{-2}s^{-1} during daytime and -37.8 pmol m^{-2}s^{-1}and 9.2 pmol m^{-2}s^{-1} during nighttime. We observed a net release of COS at the field site 11.2 % of the time. The net CO$_2$ fluxes ranged from -20.4 to 4.8 μmol m^{-2}s^{-1} and -30.3 to 36.4 μmol m^{-2}s^{-1} for 80% of all observation during day and nighttime, with daytime net emissions occurring after the cuttings of the grassland (Fig. 2 a-c and Fig. 5 a). While the COS nighttime fluxes remained unaffected by the cuts (Fig. 5 c), the daytime fluxes showed a high variability (see Fig. 5 b). Especially after the cuts we observed a strong decline in COS uptake (Fig. 4 b) and the grassland even turned into a net source for COS in middays (Fig. 2 a-c) with a highest emission flux of 26.8 pmol m^{-2}s^{-1} (midday median) in August after the cut. We observed COS emissions for up to 8 days after the cut, when the dried litter had already been removed (Fig. 2 a-c). Compared to respiration processes outpacing GPP almost instantaneously after the cuts, the grassland reached its peak COS emission on the day of the cut only in July, whereas the peak was reached five days after the cut in June and August (Fig. 2 a-c). The cut in October led to a reduction in COS uptake, which declined across several days and did not recover, as the end of the season was reached (Fig. 2 d & Fig. 5 b). After the fertilization of the field in October the grassland also turned into a source for COS during midday hours for one day (Fig. 5 b). Our flux measurements also included a time when the grassland was covered with snow (on May 20, 2015), which reduced the COS (and CO$_2$) fluxes to values close to zero. Over the course of the season, we observed a decline in the magnitude of the daytime COS uptake from -50.6 ± 24.6 pmol m^{-2}s^{-1} during midday in the first week of May down to -10.3 ± 10.4 pmol m^{-2}s^{-1} in the last week of October, which was also correlated with the decline in the CO$_2$ sink strength from -19.9 ± 8.0 μmol m^{-2}s^{-1} to -4.4 ± 1.5 μmol m^{-2}s^{-1} (Fig. 5 a-b). We observed an increase in COS and CO$_2$ fluxes within the growing phases after the cuts only up to an LAI of ~ 4 (-) (Fig. S4-S5), which then levelled out for COS and declined for CO$_2$ due to ecosystem respiration compensating GPP.

10
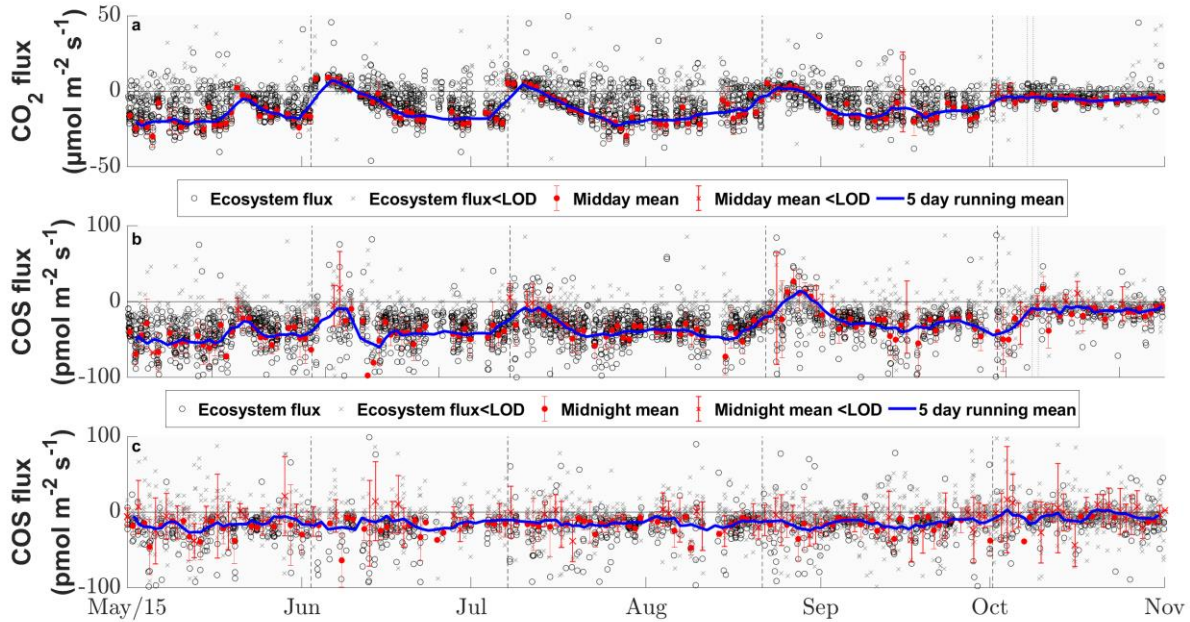
Figure 5: Seasonal cycle of the half hourly CO_2 (a), COS daytime (b) and COS nighttime (c) ecosystem fluxes in µmol m^{-2}s^{-1} and pmol m^{-2}s^{-1} depicted by black circles if they are above the limit of detection (LOD) and grey x's if they are below (Langford et al., 2015). The red circles depict the mean fluxes between 11 a.m. and 2 p.m. CET for (a & b) and between 11 p.m. and 2 a.m. for (c) that are above the LOD, while the red x's indicate means below the LOD. The red error bars depict the ±1standard deviation of the mean. The blue lines depict the running mean (5 days) for the mean fluxes. The black dashed lines depict the cuttings of the grassland.

The seasonal pattern of a decrease in COS sink strength was similar for nighttime fluxes (-18.0± 29.6 pmol m^{-2}s^{-1} to -10.6 ± 18.2 pmol m^{-2}s^{-1}) (Fig. 5c). The mean nighttime respiration also decreased over the course of the season from 15.9 ± 28.2 µmol m^{-2}s^{-1} to 9.4 ± 17.5 µmol m^{-2}s^{-1} between May and October (Fig. 5a).

Periods between May and August of low (after cuts) and high (before cuts) LAI were compared as diel courses (Fig. 5). Over the course of the day, both periods were characterized by a mean uptake of COS (Fig 6 c & d). Even though the uptake was similar during nighttime, the daytime pattern differed considerably. The modelled contribution of the soil to the ecosystem scale COS flux under high LAI conditions (Fig. 6 d) was minor, contributing between 1.3 % and 5.5/5.7 % of the ecosystem flux during midday and morning/evening, respectively. In contrast, during low LAI conditions the soil contribution to the ecosystem fluxes increased during daytime and contributed up to 82.4% of the mean hourly COS ecosystem flux (Fig 6. c). While the grassland acted as a stronger sink for COS during daytime at a high LAI, reaching peak mean uptake values of up to -41.8 pmol m^{-2}s^{-1}± 16.8 pmol m^{-2}s^{-1} during midday, the mean daytime sink strength weakened and we observed close to zero fluxes during midday in periods of low LAI. The magnitude of the soil flux (2 ± 1 pmol m^{-2}s^{-1}) was not high enough to explain the difference of up to 26.0 pmol m^{-2}s^{-1} between the measured COS ecosystem flux and COS flux resulting from the FP+ model (Fig 6 c), suggesting a missing COS source. For phases of high LAI we saw a good agreement between hourly averaged modelled and measured COS ecosystem fluxes (Fig 6 d). While the grassland acted as a net sink for CO_2 during periods of high LAI (Fig. 6 b), a combination of a decline in GPP and an increase in daytime RECO, as more incoming radiation was heating the soil surface, turned it into a net source during midday in periods of low LAI (Fig. 6 a).
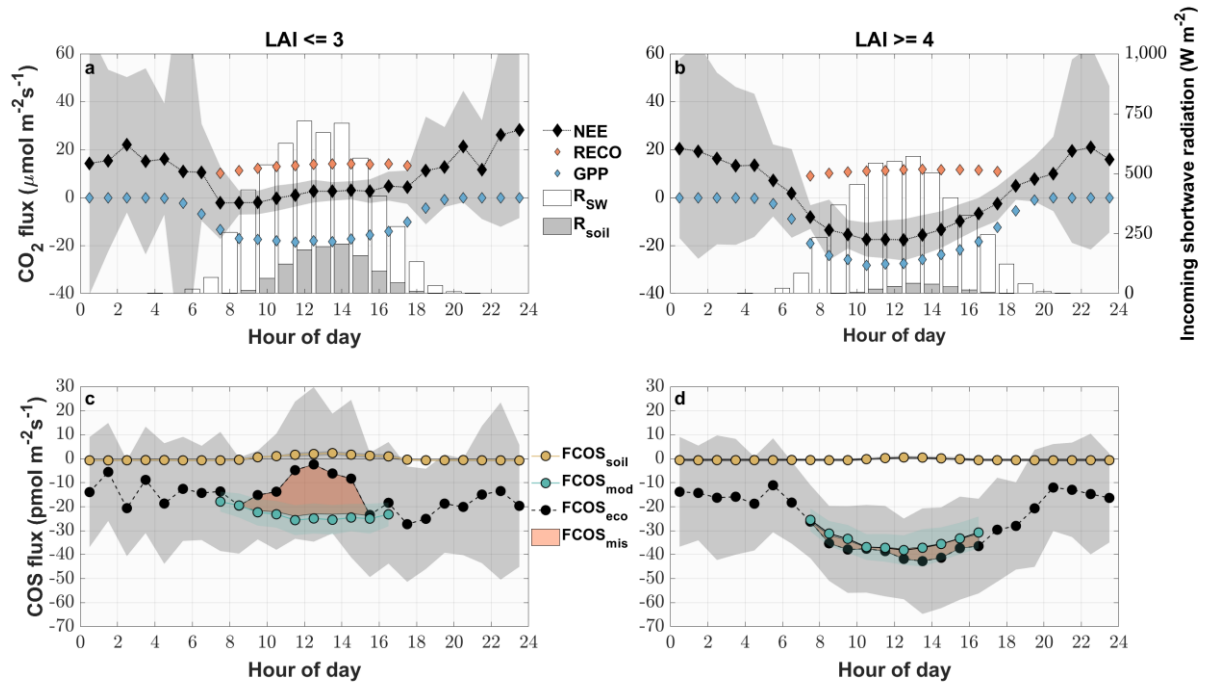
Figure 6. Mean diel variation of the measured and modelled CO_2 (a & b) and COS (c & d) fluxes for phases of low (LAI <=3) (a & c) and high (LAI >= 4) (b & d) from May to August. The carats depict the modelled gross primary productivity (blue), the modelled ecosystem respiration (red) and the measured CO_2 ecosystem fluxes (black) in μmol m^{-2}s^{-1}. The circles depict the modelled COS soil flux (yellow), the modelled COS ecosystem flux (turquoise) and the measured COS ecosystem fluxes (black) in pmol m^{-2}s^{-1}. The red area depicts the difference between the measured ecosystem flux and the sum of the modelled fluxes. The grey areas depict the ±1 standard deviation of the mean for all the measured fluxes. The white bars depict the diel mean total incoming shortwave radiation (W m^{-2}) while the grey bars indicate the diel mean shortwave radiation reaching the soil surface.

3.5 Leaf and ecosystem relative uptake

The LRU at high-light conditions, ι, which we calculated using the FP+ algorithm increased from relatively stable precut levels of 0.9-1. (-) before the 2nd and the 1st cut to up to 1.6 (-) after the 4th cut (Fig. 7a). After the decrease in ι between the 2nd and the 3rd cut, ι increased steadily until the 4th cut, with the 3rd cut seemingly not having an effect. The reason for the increase in ι after the 2nd and 4th cut was a stronger decrease in GPP than the COS uptake, while both decreased more evenly after the 3rd cut (Fig. 7b). We observed ι in the period before the 4th cut to be influenced not only by a decrease in COS uptake, but also by a decrease in COS mole fraction (Fig 7b). The mean midday ERUs varied between 2.0 ± 0.1(-) before and 4.5 ± 0.4 (-) after the cuts. The larger difference between the ERU and ι after the cuts reflect that we observed similar respiration rates at low and high LAI (Fig 6a-b).

Under low light conditions, the LRU increased during pre- and post-cut phases in a similar manner with the last 15-day period in October showing an earlier increase in the morning and evening (see Fig. S7).
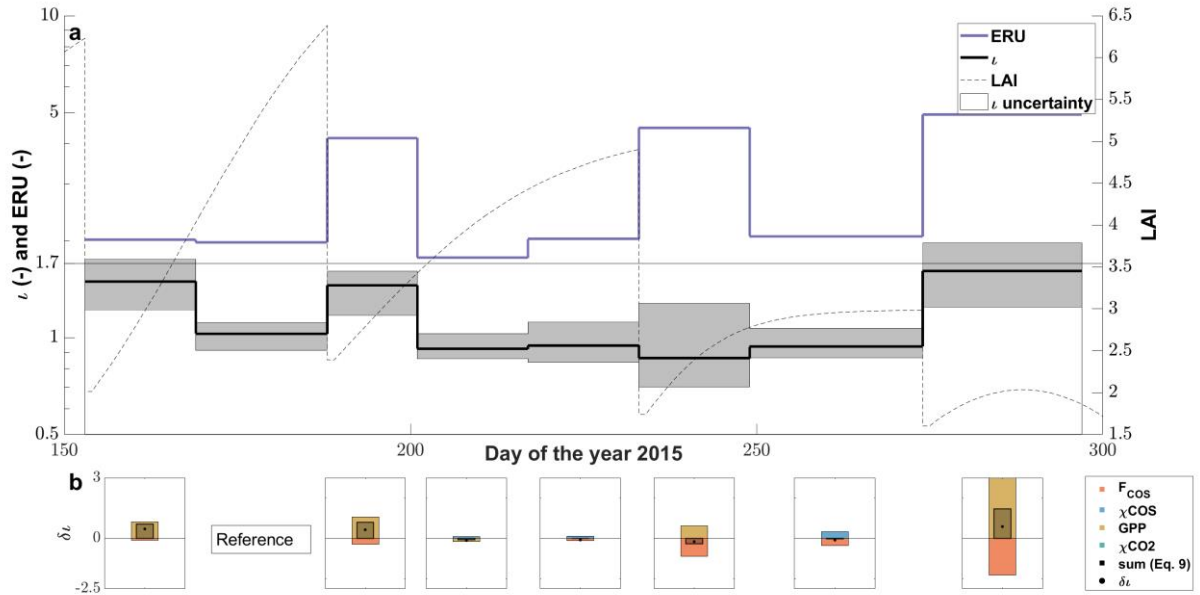
Figure 7. (a) The seasonal cycle of ɩ (black line) with the 95% confidence interval (gray area) resulting from the FP+ model and the midday mean (11 a.m. – 2 p.m. at PAR > 800 μmol m_{-2} s_{-1}) ecosystem relative uptake (ERU) (blue line) using the CO_2 ecosystem flux for the calculation windows (~15 days adjusted to cuts). The dashed black line depicts the progression of the leaf area index (LAI) of the grassland. (b) The contribution of the drivers (F_{COS}, χ_{COS}, GPP and χ_{CO2}) to the changes in ɩ between all calculation windows and the reference period (DOY 169-188) resulting from the linear perturbation analysis compared to the observed change in ɩ (δɩ).

4 Discussion

4.1 COS mole fractions

The continuous seasonal decrease in above-canopy χ_{COS} was within the range of published records observing mole fractions to decrease from 465 (in summer) to 375 ppt (in winter) (Kuhn et al., 1999). This pattern is typical for the northern hemisphere and the COS drawdown by terrestrial ecosystems (Montzka et al., 2007). We found the lowest χ_{COS} at the end of September, which coincides with the lowest ambient mole fractions of COS, measured in Ireland, the closest COS observation site Mace Head (MHD) of NOAA, on the 6th of October (Fig. S6).

The extremely low COS canopy mole fractions we observed within the canopy, have also been reported by Rastogi et al. (2018), who measured a mean χ_{COS} minimum of 152 ppt at 1 m above the soil within an old growth forest. Compared to the consistent decrease of COS below the canopy level during day and nighttime, the gradient for CO_2 reverses during nighttime due to ongoing respiration processes while plants are not photosynthetically active. Even though the COS mole fraction at the layer closest to the soil were higher during day than during nighttime, the absolute decrease in COS was lower during nighttime due to partial stomatal closure (Kooijmans et al., 2017;Campbell et al., 2017). The absolute difference in concentrations during day and nighttime originate from changes in the height of the planetary boundary layer (PBL). While the PBL is shallow during nighttime and the COS mole fraction decreases due to sink strength of the grassland, at the onset of the day, the PBL layer height increases fast and COS rich air is transported down to the ecosystem (Fig. S12) (Campbell et al., 2017). A similar steep increase until midday has also been observed by Rastogi et al. (2018). Even though CO_2 and COS share a similar pathway into plants, reflected by their respective decrease in the mole fractions within the canopy, we saw a difference at the lower levels of our gradient analysis during daytime. We only observed an increase in CO_2 mole fractions, caused by the release of CO_2 through respiration processes in the soil, whereas COS mole fractions further declined down to the soil surface. This supports our soil model, which predicted only minor COS fluxes under conditions of high LAI, when only a small portion of incident radiation reaches the soil surface.

4.2 Soil fluxes

The nighttime soil chamber measurements compare well in terms of magnitude with the COS fluxes resulting from studies using dark chambers in agricultural and grassland sites (Whelan et al., 2018;Maseyk et al., 2014;Whelan and Rhew, 2016;Liu et al., 2010) and indicate the soil to be a small sink for COS. The current understanding of COS soil exchange links the COS consumption to soil biota e.g. bacteria and fungi, possessing the ubiquitous enzyme CA (Kesselmeier et al., 1999;Meredith et al., 2019). The origin of COS in soils on the other hand is still highly debated, but comparisons of untreated and sterilized soils suggest yet unknown abiotic processes (Meredith et al., 2019;Kitz et al., 2019).

The high COS emissions resulting from the soil chambers during daytime lie at the upper end of recently stated values of agricultural and grassland sites (Whelan et al., 2018;Kitz et al., 2017;Maseyk et al., 2014;Liu et al., 2010). Partly, this can be attributed to the type of chambers we used and their deployment. We allowed the full spectrum of incoming radiation to reach the soils surface, whereas most other studies used dark chambers. Therefore we were able to capture the influence of COS emission processes coupled to thermo- and photo production on our COS soil fluxes (Whelan and Rhew, 2015;Kitz et al., 2019;Meredith et al., 2018). This also led to lower peak soil emissions of COS at the end of the season, when the incoming radiation declined.

The low COS mole fractions observed in the lowermost canopy layers just above the soil surface emphasize the importance of using air from within the canopy for soil chamber measurements and not COS richer air from above the canopy, which would increase the COS gradient and thus increase the uptake/decrease emission of COS to/from the soil.

Our modelled COS soil fluxes peak at about 12% of the maximum emissions retrieved from the soil chambers. This is owed to the difference in incident radiation reaching the soil surface between the fluxes resulting from chamber measurements and our model. For the chambers, the aboveground biomass was removed, whereas our modelled fluxes were adjusted for undisturbed canopy conditions.

Another factor contributing to the high COS soil emissions might be the yearly fertilization using slurry, as high nitrogen content in soils has been linked to a higher source strength of COS (Kaisermann et al., 2018). This agrees well with the study of Kitz et al. (2019), who found a correlation between increased soil nitrogen content and soil COS emission in a laboratory experiment with samples taken from the grassland at two different dates (i.e. June and September).

4.3 Ecosystem fluxes

Our observations show that the agriculturally used grassland acted as a major sink for COS during the growing season. The fluxes fit well within or even exceeded the COS uptake rates of published grassland and agricultural sites during their growing phases (Billesbach et al., 2014;Whelan and Rhew, 2016;Geng and Mu, 2004). The late snow event that occurred in the peak growing season almost completely inhibited the exchange of CO_2 and COS, as the snow acted as a diffusion barrier for these compounds (Björkman et al., 2010).

The cuttings and the consecutive drying of the above ground plant material at the site had a major influence on the COS exchange. COS emissions of a similar magnitude have also been reported at agricultural fields in phases of senescence (Maseyk et al., 2014;Billesbach et al., 2014). Although the soil was a strong source for COS, caused by the high R_{soil} and T_{soil} (Whelan and Rhew, 2015;Kitz et al., 2019;Meredith et al., 2018), and the sink strength of the grassland was low due to the reduced aboveground biomass, soil fluxes did not explain the emission on ecosystem level (see Fig. 6a). As plants contain precursors involved in COS emission processes, e.g. methionine and cysteine (Meredith et al., 2018), the plant litter and dying plant parts remaining at the site after the cuts might be the missing source of COS. Laboratory tests of the soil of the grassland have shown that a mixing of dried litter and soil lead to a strong but short-lived emission peak of COS (Kitz et al., 2019). We did not observe strong COS emissions after the last cut, as the incoming solar radiation, which we hypothesize to amplify the degradation of sulfur containing compounds of plants, was reduced at the end of the season. Alternatively, the

441 cutting of the grassland might induce stress mediated COS production in the remaining living plant parts (Bloem et al.,
442 2012;Gimeno et al., 2017). The delay in the peak COS emissions at ecosystem scale after the cuts could indicate that some
443 yet unknown biotic or abiotic processes take several days to release COS.

444 The short-lived COS emission by yet unknown biotic or abiotic processes after the fertilization of the grassland towards the
445 end of the growing season was likely triggered by the increase of available nitrogen (Kaisermann et al., 2018) and COS
446 precursors introduced to the soil in the form of cattle slurry (Hörtnagl et al., 2018).

447 Due to the independence of CA to catalyze COS without R_{PAR} (Stimler et al., 2011), the grassland remained a sink for COS
448 during nighttime. Again, the soil sink was too small to explain the total COS exchange (Fig. 6), which indicates that the plant
449 stomata were not fully closed (Kooijmans et al., 2017) and were responsible for the majority of the COS uptake. The
450 minimum or residual stomatal conductances at the field site in Neustift have been reported to be between 10 and 65 mmol m^{-}
451 ^{2} s^{-1} depending on the species (Wohlfahrt, 2004).

452 The large variability in COS nighttime fluxes (Fig. 5c) is due to the combination of low wind speeds and stable stratification,
453 which results in highly intermittent CO_2 (Wohlfahrt et al., 2005) and COS fluxes compared to daytime. On half-hourly basis,
454 even a nighttime net uptake of CO_2 has been reported at the field site, which is typically compensated for by large CO_2
455 emissions in a subsequent averaging period (Wohlfahrt et al., 2005). We also observed this pattern for COS.

456 Although we observed phases of high VPD and low SWC (Fig. 1), they did not lead to a decrease in CO_2 and COS
457 ecosystem fluxes (Fig. S1-S2), which has already been observed for the grasslands CO_2 and H_2O fluxes between 2001 and
458 2009. The species located at the site were insensitive to progressive drought conditions (Brilli et al., 2011).

459

4.4 LRU

461 The parameter ι of this study is placed at the lower end of a recent compilation of published leaf-level LRUs, that put 95% of
462 all data between 0.7 (-) and 6.2 (-) with a median of 1.7 (-) (Whelan et al., 2018) and also lower than the LRU of 2.53 (-)
463 estimated for grasslands by Seibt et al. (2010). Even the higher ι after the cuts was low compared to these studies. The
464 seasonal trend of ι was strongly influenced by the cutting of the grass and can be attributed mainly to changes in the ratio of
465 COS uptake to GPP. However, we also observed a strong decline in the ambient mole fraction of COS, which also had an
466 equally strong influence on the change in ι as the COS flux for the 15 day window before the last cut (Fig 7 b).

467 Even though the changes in ι can be explained, it is important to keep in mind that the grassland was a source for COS on
468 ecosystem level after the cuts. For the calculation of LRUs we had to remove the canopy flux data containing COS and/or
469 CO_2 emissions since they would yield negative values for ERU and LRU (see Eq.8). This indicates that the unknown source
470 strength after cuts likely decreases the post-cut ι's.

5 Conclusion

472 Due to the management interventions at the grassland site, the leaf area development was decoupled from seasonal changes
473 in environmental forcing. This allowed us to measure concurrent CO_2 and COS fluxes at soil and ecosystem level for
474 multiple growing periods within one season. The LAI on seasonal scale as well as incoming solar radiation on hourly to
475 seasonal scales determined whether soils were a source or a sink for COS. The incoming shortwave radiation reaching the
476 soil surface had a decisive influence on the COS soil surface flux and thus supports our hypothesis H4. The covariance
477 between the daytime CO_2 and COS fluxes on daily to seasonal level was high and the fluxes only diverged after the cuts,
478 leading to higher LRUs. Beside the perturbations of the ecosystem, the sink strength of the grassland was high for COS and
479 declined over the course of the season (H1). The COS emissions at ecosystem scale shortly after the cuts, which could not be
480 explained by the soil source, raise questions about other unknown mechanisms of COS production within ecosystems (H2).

481 With the exception of short periods after the cuts, the LRUs under high light conditions were relatively constant during the

482 season, indicating a good correlation between the COS flux and GPP under stable conditions (H3).

483 **6. Data availability**

484 Data and materials availability: https://doi.org/10.5281/zenodo.3886554

485 **7. Author contributions**

486 Felix M. Spielmann: Data curation, Formal analysis, Investigation, Methodology, Software, Visualization, Writing – original

487 draft

488 Albin Hammerle: Data curation, Investigation, Software, Writing – original draft

489 Florian Kitz: Data curation, Formal analysis, Investigation, Methodology, Software, Writing – original draft

490 Katharina Gerdel: Investigation, Software, Writing – original draft

491 Georg Wohlfahrt: Conceptualization, Funding acquisition, Investigation, Methodology, Project administration, Software,

492 Supervision, Writing – original draft

493 **8. Competing interests**

494 The authors declare no competing financial interests.

495 **9. Acknowledgements**

483 **10. References**

504 Asaf, D., Rotenberg, E., Tatarinov, F., Dicken, U., Montzka, S. A., and Yakir, D.: Ecosystem photosynthesis inferred from
505   measurements of carbonyl sulphide flux, Nature Geoscience, 6, 186-190, 10.1038/ngeo1730, 2013.
506 Aubinet, M., Grelle, A., Ibrom, A., Rannik, Ü., Moncrieff, J., Foken, T., Kowalski, A. S., Martin, P. H., Berbigier, P.,
507   Bernhofer, C., Clement, R., Elbers, J., Granier, A., Grünwald, T., Morgenstern, K., Pilegaard, K., Rebmann, C.,
508   Snijders, W., Valentini, R., and Vesala, T.: Estimates of the Annual Net Carbon and Water Exchange of Forests:
509   The EUROFLUX Methodology, in: Advances in Ecological Research Volume 30, edited by: Fitter, A. H., and
510   Raffaelli, D. G., Advances in Ecological Research, Academic Press, 113-175, 1999.
511 Baldocchi, D.: Measuring fluxes of trace gases and energy between ecosystems and the atmosphere - the state and future of
512   the eddy covariance method, Glob Chang Biol, 20, 3600-3609, doi.org/10.1111/gcb.12649, 2014.
513 Barr, A. G., Richardson, A. D., Hollinger, D. Y., Papale, D., Arain, M. A., Black, T. A., Bohrer, G., Dragoni, D., Fischer, M.
514   L., Gu, L., Law, B. E., Margolis, H. A., McCaughey, J. H., Munger, J. W., Oechel, W., and Schaeffer, K.: Use of
515   change-point detection for friction-velocity threshold evaluation in eddy-covariance studies, Agricultural and Forest
516   Meteorology, 171, 31-45, 10.1016/j.agrformet.2012.11.023, 2013.
517 Billesbach, D. P., Berry, J. A., Seibt, U., Maseyk, K., Torn, M. S., Fischer, M. L., Abu-Naser, M., and Campbell, J. E.:
518   Growing season eddy covariance measurements of carbonyl sulfide and CO2 fluxes: COS and CO2 relationships in
519   Southern Great Plains winter wheat, Agricultural and Forest Meteorology, 184, 48-55,
520   10.1016/j.agrformet.2013.06.007, 2014.

Björkman, M. P., Morgner, E., Cooper, E. J., Elberling, B., Klemedtsson, L., and Björk, R. G.: Winter carbon dioxide effluxes from Arctic ecosystems: An overview and comparison of methodologies, Global Biogeochemical Cycles, 24, 10.1029/2009gb003667, 2010.

Bloem, E., Haneklaus, S., Kesselmeier, J., and Schnug, E.: Sulfur Fertilization and Fungal Infections Affect the Exchange of H2S and COS from Agricultural Crops, Journal of Agricultural and Food Chemistry, 60, 7588-7596, 10.1021/jf301912h, 2012.

Brilli, F., Hörtnagl, L., Hammerle, A., Haslwanter, A., Hansel, A., Loreto, F., and Wohlfahrt, G.: Leaf and ecosystem response to soil water availability in mountain grasslands, Agricultural and Forest Meteorology, 151, 1731-1740, doi.org/10.1016/j.agrformet.2011.07.007, 2011.

Brühl, C., Lelieveld, J., Crutzen, P. J., and Tost, H.: The role of carbonyl sulphide as a source of stratospheric sulphate aerosol and its impact on climate, Atmos. Chem. Phys., 12, 1239-1253, 10.5194/acp-12-1239-2012, 2012.

Campbell, J. E., Whelan, M. E., Berry, J. A., Hilton, T. W., Zumkehr, A., Stinecipher, J., Lu, Y., Kornfeld, A., Seibt, U., Dawson, T. E., Montzka, S. A., Baker, I. T., Kulkarni, S., Wang, Y., Herndon, S. C., Zahniser, M. S., Commane, R., and Loik, M. E.: Plant Uptake of Atmospheric Carbonyl Sulfide in Coast Redwood Forests, Journal of Geophysical Research-Biogeosciences, 122, 3391-3404, 10.1002/2016jg003703, 2017.

Ensign, S. A.: Reactivity of Carbon Monoxide Dehydrogenase from Rhodospirillum rubrum with Carbon Dioxide, Carbonyl Sulfide, and Carbon Disulfide, Biochemistry, 34, 5372-5381, 10.1021/bi00016a008, 1995.

Geng, C., and Mu, Y.: Carbonyl sulfide and dimethyl sulfide exchange between lawn and the atmosphere, Journal of Geophysical Research: Atmospheres, 109, 10.1029/2003jd004492, 2004.

Gerdel, K., Spielmann, F. M., Hammerle, A., and Wohlfahrt, G.: Eddy covariance carbonyl sulfide flux measurements with a quantum cascade laser absorption spectrometer, Atmospheric Measurement Techniques, 10, 3525-3537, 10.5194/amt-10-3525-2017, 2017.

Gimeno, T. E., Ogee, J., Royles, J., Gibon, Y., West, J. B., Burlett, R., Jones, S. P., Sauze, J., Wohl, S., Benard, C., Genty, B., and Wingate, L.: Bryophyte gas-exchange dynamics along varying hydration status reveal a significant carbonyl sulphide (COS) sink in the dark and COS source in the light, New Phytologist, 215, 965-976, 10.1111/nph.14584, 2017.

Hortnagl, L., Clement, R., Graus, M., Hammerle, A., Hansel, A., and Wohlfahrt, G.: Dealing with disjunct concentration measurements in eddy covariance applications: A comparison of available approaches, Atmospheric Environment, 44, 2024-2032, 10.1016/j.atmosenv.2010.02.042, 2010.

Hörtnagl, L., Barthel, M., Buchmann, N., Eugster, W., Butterbach-Bahl, K., Díaz-Pinés, E., Zeeman, M., Klumpp, K., Kiese, R., Bahn, M., Hammerle, A., Lu, H., Ladreiter-Knauss, T., Burri, S., and Merbold, L.: Greenhouse gas fluxes over managed grasslands in Central Europe, Global Change Biology, 24, 1843-1872, 10.1111/gcb.14079, 2018.

Kaisermann, A., Jones, S., Wohl, S., Ogée, J., and Wingate, L.: Nitrogen Fertilization Reduces the Capacity of Soils to Take up Atmospheric Carbonyl Sulphide, Soil Syst., 2, 10.3390/soilsystems2040062, 2018.

Kesselmeier, J., Teusch, N., and Kuhn, U.: Controlling variables for the uptake of atmospheric carbonyl sulfide by soil, J. Geophys. Res.-Atmos., 104, 11577-11584, 10.1029/1999jd900090, 1999.

Kitz, F., Gerdel, K., Hammerle, A., Laterza, T., Spielmann, F. M., and Wohlfahrt, G.: In situ soil COS exchange of a temperate mountain grassland under simulated drought, Oecologia, 1-10, 10.1007/s00442-016-3805-0, 2017.

Kitz, F., Gómez-Brandón, M., Eder, B., Etemadi, M., Spielmann, F. M., Hammerle, A., Insam, H., and Wohlfahrt, G.: Soil carbonyl sulfide exchange in relation to microbial community composition: Insights from a managed grassland soil amendment experiment, Soil Biology and Biochemistry, 135, 28-37, 10.1016/j.soilbio.2019.04.005, 2019.

Kooijmans, L. M. J., Uitslag, N. A. M., Zahniser, M. S., Nelson, D. D., Montzka, S. A., and Chen, H. L.: Continuous and high-precision atmospheric concentration measurements of COS, CO2, CO and H2O using a quantum cascade laser spectrometer (QCLS), Atmospheric Measurement Techniques, 9, 5293-5314, 10.5194/amt-9-5293-2016, 2016.

Kooijmans, L. M. J., Maseyk, K., Seibt, U., Sun, W., Vesala, T., Mammarella, I., Kolari, P., Aalto, J., Franchin, A., Vecchi, R., Valli, G., and Chen, H.: Canopy uptake dominates nighttime carbonyl sulfide fluxes in a boreal forest, Atmos. Chem. Phys., 17, 11453-11465, 10.5194/acp-17-11453-2017, 2017.

Kooijmans, L. M. J., Sun, W., Aalto, J., Erkkilä, K. M., Maseyk, K., Seibt, U., Vesala, T., Mammarella, I., and Chen, H.: Influences of light and humidity on carbonyl sulfide-based estimates of photosynthesis, Proc Natl Acad Sci U S A, 10.1073/pnas.1807600116, 2019.

Krysztofiak, G., Té, Y. V., Catoire, V., Berthet, G., Toon, G. C., Jégou, F., Jeseck, P., and Robert, C.: Carbonyl Sulphide (OCS) Variability with Latitude in the Atmosphere, Atmosphere-Ocean, 53, 89-101, 10.1080/07055900.2013.876609, 2015.

Kuhn, U., Ammann, C., Wolf, A., Meixner, F. X., Andreae, M. O., and Kesselmeier, J.: Carbonyl sulfide exchange on an ecosystem scale: soil represents a dominant sink for atmospheric COS, Atmospheric Environment, 33, 995-1008, Doi 10.1016/S1352-2310(98)00211-8, 1999.

Langford, B., Acton, W., Ammann, C., Valach, A., and Nemitz, E.: Eddy-covariance data with low signal-to-noise ratio: time-lag determination, uncertainties and limit of detection, Atmospheric Measurement Techniques, 8, 4197-4213, 10.5194/amt-8-4197-2015, 2015.

Lasslop, G., Reichstein, M., Papale, D., Richardson, A. D., Arneth, A., Barr, A., Stoy, P., and Wohlfahrt, G.: Separation of net ecosystem exchange into assimilation and respiration using a light response curve approach: critical issues and global evaluation, Global Change Biology, 16, 187-208, 10.1111/j.1365-2486.2009.02041.x, 2010.

Le Quere, C., Andrew, R. M., Friedlingstein, P., Sitch, S., Pongratz, J., Manning, A. C., Korsbakken, J. I., Peters, G. P., Canadell, J. G., Jackson, R. B., Boden, T. A., Tans, P. P., Andrews, O. D., Arora, V. K., Bakker, D. C. E., Barbero,

L., Becker, M., Betts, R. A., Bopp, L., Chevallier, F., Chini, L. P., Ciais, P., Cosca, C. E., Cross, J., Currie, K., Gasser, T., Harris, I., Hauck, J., Haverd, V., Houghton, R. A., Hunt, C. W., Hurtt, G., Ilyina, T., Jain, A. K., Kato, E., Kautz, M., Keeling, R. F., Goldewijk, K. K., Kortzinger, A., Landschutzer, P., Lefevre, N., Lenton, A., Lienert, S., Lima, I., Lombardozzi, D., Metzl, N., Millero, F., Monteiro, P. M. S., Munro, D. R., Nabel, J., Nakaoka, S., Nojiri, Y., Padin, X. A., Peregon, A., Pfeil, B., Pierrot, D., Poulter, B., Rehder, G., Reimer, J., Rodenbeck, C., Schwinger, J., Seferian, R., Skjelvan, I., Stocker, B. D., Tian, H. Q., Tilbrook, B., Tubiello, F. N., van der Laan-Luijkx, I. T., van der Werf, G. R., van Heuven, S., Viovy, N., Vuichard, N., Walker, A. P., Watson, A. J., Wiltshire, A. J., Zaehle, S., and Zhu, D.: Global Carbon Budget 2017, Earth System Science Data, 10, 405-448, 10.5194/essd-10-405-2018, 2018.

Liaw, A., and Wiener, M.: Classification and Regression by RandomForest, R News, 2/3, 18-22, 2002.

Liu, J., Geng, C., Mu, Y., Zhang, Y., Xu, Z., and Wu, H.: Exchange of carbonyl sulfide (COS) between the atmosphere and various soils in China, Biogeosciences, 7, 753-762, 10.5194/bg-7-753-2010, 2010.

Lorimer, G. H., and Pierce, J.: Carbonyl sulfide: an alternate substrate for but not an activator of ribulose-1,5-bisphosphate carboxylase, The Journal of biological chemistry, 264, 2764-2772, 1989.

Maseyk, K., Berry, J. A., Billesbach, D., Campbell, J. E., Torn, M. S., Zahniser, M., and Seibt, U.: Sources and sinks of carbonyl sulfide in an agricultural field in the Southern Great Plains, Proceedings of the National Academy of Sciences of the United States of America, 111, 9064-9069, 10.1073/pnas.1319132111, 2014.

Meredith, L. K., Boye, K., Youngerman, C., Whelan, M., Ogee, J., Sauze, J., and Wingate, L.: Coupled Biological and Abiotic Mechanisms Driving Carbonyl Sulfide Production in Soils, Soil Syst., 2, 27, 10.3390/soilsystems2030037, 2018.

Meredith, L. K., Ogée, J., Boye, K., Singer, E., Wingate, L., von Sperber, C., Sengupta, A., Whelan, M., Pang, E., Keiluweit, M., Brüggemann, N., Berry, J. A., and Welander, P. V.: Soil exchange rates of COS and CO18O differ with the diversity of microbial communities and their carbonic anhydrase enzymes, The ISME Journal, 13, 290-300, 10.1038/s41396-018-0270-2, 2019.

Montzka, S. A., Calvert, P., Hall, B. D., Elkins, J. W., Conway, T. J., Tans, P. P., and Sweeney, C.: On the global distribution, seasonality, and budget of atmospheric carbonyl sulfide (COS) and some similarities to CO2, J. Geophys. Res.-Atmos., 112, 10.1029/2006jd007665, 2007.

Notni, J., Schenk, S., Protoschill-Krebs, G., Kesselmeier, J., and Anders, E.: The missing link in COS metabolism: a model study on the reactivation of carbonic anhydrase from its hydrosulfide analogue, Chembiochem : a European journal of chemical biology, 8, 530-536, 10.1002/cbic.200600436, 2007.

Ogawa, T., Noguchi, K., Saito, M., Nagahata, Y., Kato, H., Ohtaki, A., Nakayama, H., Dohmae, N., Matsushita, Y., Odaka, M., Yohda, M., Nyunoya, H., and Katayama, Y.: Carbonyl Sulfide Hydrolase from Thiobacillus thioparus Strain THI115 Is One of the β-Carbonic Anhydrase Family Enzymes, Journal of the American Chemical Society, 135, 3818-3825, 10.1021/ja307735e, 2013.

Protoschill-Krebs, G., and Kesselmeier, J.: ENZYMATIC PATHWAYS FOR THE CONSUMPTION OF CARBONYL SULFIDE (COS) BY HIGHER-PLANTS, Botanica Acta, 105, 206-212, 1992.

Rastogi, B., Berkelhammer, M., Wharton, S., Whelan, M. E., Itter, M. S., Leen, J. B., Gupta, M. X., Noone, D., and Still, C. J.: Large Uptake of Atmospheric OCS Observed at a Moist Old Growth Forest: Controls and Implications for Carbon Cycle Applications, Journal of Geophysical Research-Biogeosciences, 123, 3424-3438, 10.1029/2018jg004430, 2018.

Sandoval-Soto, L., Stanimirov, M., von Hobe, M., Schmitt, V., Valdes, J., Wild, A., and Kesselmeier, J.: Global uptake of carbonyl sulfide (COS) by terrestrial vegetation: Estimates corrected by deposition velocities normalized to the uptake of carbon dioxide (CO_2), Biogeosciences, 2, 125-132, 10.5194/bg-2-125-2005, 2005.

Seefeldt, L. C., Rasche, M. E., and Ensign, S. A.: Carbonyl sulfide and carbon dioxide as new substrates, and carbon disulfide as a new inhibitor, of nitrogenase, Biochemistry, 34, 5382-5389, 10.1021/bi00016a009, 1995.

Seibt, U., Kesselmeier, J., Sandoval-Soto, L., Kuhn, U., and Berry, J.: A kinetic analysis of leaf uptake of COS and its relation to transpiration, photosynthesis and carbon isotope fractionation, Biogeosciences, 7, 333-341, 2010.

Smeulders, M. J., Pol, A., Venselaar, H., Barends, T. R. M., Hermans, J., Jetten, M. S. M., and Op den Camp, H. J. M.: Bacterial CS$_2$ Hydrolases from Acidithiobacillus thiooxidans Strains Are Homologous to the Archaeal Catenane CS$_2$ Hydrolase, Journal of Bacteriology, 195, 4046, 10.1128/JB.00627-13, 2013.

Spielmann, F. M., Wohlfahrt, G., Hammerle, A., Kitz, F., Migliavacca, M., Alberti, G., Ibrom, A., El-Madany, T. S., Gerdel, K., Moreno, G., Kolle, O., Karl, T., Peressotti, A., and Delle Vedove, G.: Gross Primary Productivity of Four European Ecosystems Constrained by Joint CO2 and COS Flux Measurements, Geophys. Res. Lett., 0, 10.1029/2019gl082006, 2019.

Stimler, K., Berry, J. A., Montzka, S. A., and Yakir, D.: Association between Carbonyl Sulfide Uptake and (18)Delta during Gas Exchange in C-3 and C-4 Leaves, Plant Physiology, 157, 509-517, 10.1104/pp.111.176578, 2011.

Stoy, P. C., Katul, G. G., Siqueira, M. B. S., Juang, J. Y., Novick, K. A., McCarthy, H. R., Oishi, A. C., Uebelherr, J. M., Kim, H. S., and Oren, R.: Separating the effects of climate and vegetation on evapotranspiration along a successional chronosequence in the southeastern US, Global Change Biology, 12, 2115-2135, 10.1111/j.1365-2486.2006.01244.x, 2006.

Tucker, C. J.: Red and photographic infrared linear combinations for monitoring vegetation, Remote Sensing of Environment, 8, 127-150, https://doi.org/10.1016/0034-4257(79)90013-0, 1979.

649   Whelan, M. E., and Rhew, R. C.: Carbonyl sulfide produced by abiotic thermal and photodegradation of soil organic matter
650   from wheat field substrate, Journal of Geophysical Research-Biogeosciences, 120, 54-62, 10.1002/2014jg002661,
651   2015.
652   Whelan, M. E., and Rhew, R. C.: Reduced sulfur trace gas exchange between a seasonally dry grassland and the atmosphere,
653   Biogeochemistry, 128, 267-280, 10.1007/s10533-016-0207-7, 2016.
654   Whelan, M. E., Lennartz, S. T., Gimeno, T. E., Wehr, R., Wohlfahrt, G., Wang, Y., Kooijmans, L. M. J., Hilton, T. W.,
655   Belviso, S., Peylin, P., Commane, R., Sun, W., Chen, H., Kuai, L., Mammarella, I., Maseyk, K., Berkelhammer, M.,
656   Li, K. F., Yakir, D., Zumkehr, A., Katayama, Y., Ogée, J., Spielmann, F. M., Kitz, F., Rastogi, B., Kesselmeier, J.,
657   Marshall, J., Erkkilä, K. M., Wingate, L., Meredith, L. K., He, W., Bunk, R., Launois, T., Vesala, T., Schmidt, J. A.,
658   Fichot, C. G., Seibt, U., Saleska, S., Saltzman, E. S., Montzka, S. A., Berry, J. A., and Campbell, J. E.: Reviews and
659   syntheses: Carbonyl sulfide as a multi-scale tracer for carbon and water cycles, Biogeosciences, 15, 3625-3657,
660   10.5194/bg-15-3625-2018, 2018.
661   Wohlfahrt, G., Bahn, M., Tappeiner, U., and Cernusca, A.: A multi-component, multi-species model of vegetation-
662   atmosphere CO_2 and energy exchange for mountain grasslands, Agricultural and Forest Meteorology, 106, 261-
663   287, 10.1016/s0168-1923(00)00224-0, 2001.
664   Wohlfahrt, G.: Modelling fluxes and concentrations of CO_2, H_2O and sensible heat within and above a mountain meadow
665   canopy: A comparison of three Lagrangian models and three parameterisation options for the Lagrangian time
666   scale, Boundary-Layer Meteorology, 113, 43-80, 10.1023/B:BOUN.0000037326.40490.1f, 2004.
667   Wohlfahrt, G., Anfang, C., Bahn, M., Haslwanter, A., Newesely, C., Schmitt, M., Drosler, M., Pfadenhauer, J., and
668   Cernusca, A.: Quantifying nighttime ecosystem respiration of a meadow using eddy covariance, chambers and
669   modelling, Agricultural and Forest Meteorology, 128, 141-162, 10.1016/j.agrformet.2004.11.003, 2005.
670   Wohlfahrt, G., Hammerle, A., Haslwanter, A., Bahn, M., Tappeiner, U., and Cernusca, A.: Seasonal and inter-annual
671   variability of the net ecosystem CO_2 exchange of a temperate mountain grassland: Effects of weather and
672   management, Journal of Geophysical Research: Atmospheres, 113, 10.1029/2007jd009286, 2008.
673   Wohlfahrt, G., Brilli, F., Hoertnagl, L., Xu, X., Bingemer, H., Hansel, A., and Loreto, F.: Carbonyl sulfide (COS) as a tracer
674   for canopy photosynthesis, transpiration and stomatal conductance: potential and limitations, Plant Cell and
675   Environment, 35, 657-667, 10.1111/j.1365-3040.2011.02451.x, 2012.
676   Yang, F., Qubaja, R., Tatarinov, F., Rotenberg, E., and Yakir, D.: Assessing canopy performance using carbonyl sulfide
677   measurements, Global Change Biology, 24, 3486-3498, doi:10.1111/gcb.14145, 2018.
678